AUTOMATIC REGISTRATION METHOD FOR THE EVALUATION OF POST SURGICAL BONY MINERALIZATION

G. Mañana, E. Romero

{*gjmananag,edromero*}*@unal.edu.co*
BioIngenium Research Group
National University
Bogotá, Colombia

M. E. Forero

marthafor@gmail.com
Colombian Dental Federation
Santo Tomás University
Bogotá, Colombia

ABSTRACT

Digital subtraction is a common technique used in radiographic studies of periapical lesions and other dental disorders, for which the treatment must be evaluated over time. This paper presents a fast and reliable parallel image registration method for subtracting two digitized radiographs where an unpredicted mismatch is present. An optimal affine transformation is found using an adaptive Genetic Algorithm (GA) as the optimization strategy and a correlation ratio as the similarity measure. The parallel GA implemented takes advantage of the CPU idle cycles of a computational grid, resulting in an application that exploits an existent infrastructure and with a computational time of about twenty seconds when processing pairs of standard intra-oral radiographs. By using an existing hardware infrastructure and software of free distribution, the proposed approach can be used in public hospitals and other institutions of low budget. The validation process shows that no significant differences appear between the automatic system and the manual registration. The results show that the technique of digital radiographic subtraction is a determining tool in the evaluation of post-surgical bony mineralization in endodontic surgery, in clinical environments where it is not viable to follow a standardization protocol.

Index Terms— Digital subtraction, genetic algorithms, grid computing, bony mineralization

1. INTRODUCTION

Endodontic surgery is the treatment to save a tooth when the root canal system can not be completely sealed or adequately debrided. In the development of this surgery, diseased tissue or reactive alveolar bone is removed in the lateral or periradicular region around the affected tooth [1], the root tip is prepared to be resected and finally a filling material is inserted to seal the duct [2, 3].

Evaluation of hard tissue changes after periradicular surgery requires measures of clinical and radiographic assessment. Ideally, the best estimate of the state of bone formation is exploratory surgery. However, this approach is unfeasible and that is why non-invasive radiographic measurements have become the main tool of control [4]. Obtained by sequential radiographic examinations, such measures allow determining the gain or loss of bone at the postoperative stage of apical surgeries.

Conventional radiography requires a change in the mineralization of 30-60% to become visible [5]: small changes, while clinically important, might not be detected [6, 7]. Digital subtraction is a technique that facilitates the detection of these small bone changes through the production and processing of high-resolution images [8]. Digital subtraction radiography, which by definition requires the previous alignment or "registration" of the images, was first introduced by Gröndahl et al. [9] and has proved to be more sensitive than assessment using conventional radiographs in the detection of small periradicular bone changes [10]. In comparison with conventional radiography, x-ray digitization provides a high diagnostic sensitivity and specificity, with the potential to allow numerical estimates of the disease and the cicatrization process, mainly in the mineral apposition stage [11].

The monitoring of the development of periradicular surgery is done through x-rays taken at different times. The alignment is altered mainly due to differences in patient position in relation to the radiographic cone, but also because of differences in the exposure conditions and processing of the film [10]. By registration and subsequent subtraction of radiographs taken to the same patient at different times, it is possible to detect changes in tissue, otherwise undetectable. This method has proven particularly useful in early diagnosis of bone lesions and in monitoring the evolution of pathologies [4, 9, 12]. Many authors have shown the ability of this method to increase the quality of diagnosis of proximal caries [9], periapical lesions [5] and periodontal disease, allowing an assessment of bone loss [4, 13]. In particular, radiographic subtraction has also proved useful in assessing the post-surgical bone mineralization [12].

A detection and tracking system requires, therefore, of the precise alignment of radiographs for these changes can be de-

tected. Different strategies have been proposed for the correction of geometric distortions present. These range from manual correction [14], to the use of fixation devices that ensure a consistent projection across time [15]. However, in daily clinical practice, the dentist does not have adequate fixation devices for patients, a situation that has limited the use of this method.

This article proposes a method of fully automatic registration, to be used in cases where there is a notorious misalignment. The process begins with the digitization of the X-rays photographs, where one of these will be considered the *reference image* and the other as the *floating image*. Then, lighting intensities differences are eliminated through an equalization algorithm described below. Successive transformations are next applied to the floating image, comparing at each step the resulting image with the reference image, and using this as a *similarity measure* for determining the degree of alignment. This stage uses a genetic algorithm to find the transformation that produces the optimal registration. The process has proven to be robust, reliable and reproducible for all digitized radiographs, and has proven to be able to replace manual registration.

The article is structured as follows. Next section, Section 2, presents a brief introduction to image registration, as the basis for the formulation of the problem. Section 3, Methodology, presents the proposed methodology, which includes the process of image acquisition, preprocessing, interpolation approach, similarity measure, registration method and optimization method. This section also presents the validation process for the proposed algorithm. In Section 4, the results of applying the proposed methodology are presented and analyzed, quantitatively and qualitatively. Finally, Section 5 presents a discussion on the applicability of automatic registration in radiographic subtraction problems in general, and presents some important conclusions regarding the evaluation of post-surgical bone mineralization using a system like the one proposed.

2. IMAGE REGISTRATION

The registration of medical images poses the problem of finding the geometric transformation that aligns two or more images optimally. The manual registration requires an interactive application where the expert can view digitized radiographs to register, and apply, using input devices such as mouse and keyboard, the changes needed to align them. As the expert applies different transformations, the application computes the degree of alignment or *similarity measure*. To reduce the time required for the alignment of the images, several semi-automatic methods have been developed based on markers that must appear on the radiographs to register. These points can come from a reference or fixation of the patient, or from manual selection by the expert. The first method has the obvious disadvantage of requiring additional accessories X-ray equipment standard.

To determine the optimal processing is fully automated it is necessary to first find a criterion to measure the degree of alignment between the transformed image and the image as the reference. This measurement is known as a similarity measure and there are different approaches for computing, the most robust those based on statistical principles and concepts borrowed from information theory. In this paper, the algorithm used for automatic registration used only the intensities of the pixels of the images to calculate the degree of alignment. The registration problem then is to find the geometric transformation that maximizes the function relating the possible changes with their respective measures of similarity, a feature which does not have a mathematical representation. This is an optimization problem that can be defined as finding a global maximum in a multi-parametric extremely irregular, where conventional numerical methods tend to be trapped in local extrema.

In general, any image registration technique can be described by three main components [16]:

1. A *geometrical transformation* which relates reference and template images,
2. a *similarity measure* which measures similarity between reference and transformed image,
3. an *optimization scheme* which determines the optimal transformation as a function of the similarity measure.

Geometrical transformation refers to the mathematical forms of the geometrical mapping used in the registration process and can be classified by complexity into rigid transformations, where all distances are preserved, and deformable or non-rigid transformations where images are stretched or deformed. While the first is ideal for most fusion applications, and accounts for differences such as patient positioning, non-rigid transformations are used to take into account more complex motions, such as breathing or heartbeat.

The *similarity measure* is the driving force behind the registration process, and it aims to maximize the similarity between both images. From a probabilistic point of view, it can be viewed as a likelihood term that expresses the probability of a match between the reference and transformed image [17]. Like many other problems in computer vision and image analysis, registration can be formulated as an optimization problem whose goal is to minimize an associated cost function [16]:

$$C = -C_{similarity} + C_{transformation}, \qquad (1)$$

where the first term characterizes the similarity between the images and the second term characterizes the cost associated with particular deformations. From a probabilistic point of view, the cost function in eq. (1) can be can be explained in a Bayesian context. In this framework, the similarity measure

can be viewed as a likelihood term which expresses the probability of a match between the two images, and the second term can be interpreted as a prior which represents *a priori* knowledge about the expected deformation. This term only plays a role in non-rigid registration and in the case of rigid registration is usually ignored.

Several approaches can be used to optimize this function. They go from the use of standard numerical methods to the use of evolutionary methods, including some hybrid approaches. No matter what method is used, this always implies an iterative process whose computational cost is so high that prevents most applications from performing appropriately in real time situations. One possible way to solve this issue is to devise faster algorithms. Another way is to exploit the intrinsic parallelism that most methods convey.

Medical image registration spans numerous applications and there is a large score of different techniques reported in the literature. What follows is an attempt to classify the different techniques and categorize them based upon some criteria, for a complete analysis, please refer to, e.g., [18]. Maintz and Viergever [19] originally proposed a nine-dimensional scheme that can be condensed into the following eight criteria [20]: *image dimensionality, registration basis, geometrical transformation, degree of interaction, optimization procedure, image acquisition modalities, subject,* and *object*.

Image dimensionality refers to the number of geometrical dimensions of the image spaces involved, which in medical applications are typically two and three-dimensional, but may include time as a fourth dimension. For spatial registration, there are the 2D/2D, 3D/3D and the more complex 2D/3D registration (e.g., CT/X-ray).

The *registration basis* is the aspect of the two images used to perform the registration. In this category, registration can be classified into *extrinsic* and *intrinsic* methods. Registration methods that are based upon the attachment of markers are termed extrinsic methods, and in contrast, those which rely on anatomic features only are termed intrinsic. When there are no known correspondences as input, intensity patterns in the two views are used for alignment. A basis known as *intensity*- or *voxel*-based, has become in recent years the most widely used registration basis in medical imaging. Here there are two distinct approaches: the first reduces the image gray value content to a representative set of scalars and orientations (e.g. principal axes and moments based methods), the second uses the full image pixel content throughout the registration process. In general, intensity-based methods are more complex, yet more flexible.

The category *geometrical transformation* refers to the mathematical forms of the geometrical mapping used to align points in one space with those in the other. These include *rigid transformations*, which preserve all distances, i.e., transformations that preserve the straightness of lines - and hence planarity of surfaces - and all angles between straight lines. Images are rotated and translated in two or three dimensions in the matching process, but not deformed in any way. This is ideal for most fusion applications, and accounts for differences such as patient positioning. Registration problems that are limited to rigid transformations are called *rigid registration* problems. In deformable or *non-rigid registration*, images are stretched to take into account complex motions, such as breathing, and any changes in the shape of the body or organs, which may occur following surgery, for example. Non-rigid transformations are important not only for applications to non-rigid anatomy, but also for inter-patient registration of rigid anatomy and intra-patient registration of rigid anatomy, in those cases where there are non-rigid distortions caused by the image acquisition procedure. These include *scaling transformations*, with a special case when the scaling is isotropic, known as *similarity transformations*; the more general *affine transformations* that preserve the straightness of lines and planarity of surfaces, as well as parallelism, but change the angles between lines; the even more general *projective transformations* that preserve the straightness of lines and planarity of surfaces, but no parallelism; *perspective transformations*, a subset of the projective transformations, required for images obtained by techniques such as X-ray, endoscopy or microscopy, and finally *curved transformations* which do not preserve the straightness of lines. Each type of transformation contains as special cases the ones described before it, e.g., *rigid transformations* are a special type of *non-rigid transformations*, and so on. Transformations that are applied to the whole image are called *global*, while transformations that are applied to subsections of the image are called *local*. Rigid, affine and projective transformations are generally global, and curved transformations are more or less local, depending upon the underlying physical model used.

Degree of interaction refers to the degree of intervention of a human operator in the registration algorithm. The fully automatic algorithm, which requires no user interaction and represents the ideal situation, is a central focus of the subtraction service presented in this chapter.

The *optimization procedure* is the method by which the function that measures the alignment of the images is maximized. Depending upon the mathematical approach to registration used, i.e., *parametric* or *non-parametric*, the optimization method will try to find an optimum of some function defined on the parameter space, or will try to come up with an appropriate measure, both for the similarity of the images as well as for the likelihood of a non-parametric transformation. The more common situation here is that in which a global extremum is sought among many local ones by means of iterative search. In parametric registration, popular techniques include traditional numerical methods like Powells method [21], downhill simplex [22], gradient descent methods, as well as evolutionary methods like genetic algorithms [23], simulated annealing [24], and differential evolution [25].

Modalities refers to the means by which the images to be registered are acquired. Two-dimensional images are ac-

quired, e.g., by X-ray projections captured on film or digitally, and three-dimensional images are typically acquired by tomographic modalities such as computed tomography (CT), nuclear magnetic resonance (MRI), or positron emission tomography (PET). In medical applications the object in each view is some anatomical region of the body. In all cases we are concerned primarily with digital images stored as discrete arrays of intensity values. Registration methods used for like modalities are typically distinct from those used for differing modalities. They are called *mono-modal* and *multi-modal* registration, respectively.

Subject refers to patient involvement and there can be *intra-patient* registration involving images of the same patient, *inter-patient* registration involving images of different patients, and *atlas*. Atlas refers to registration between an image acquired from a single patient and an image constructed from an image database of many patients.

Finally, *object* refers to the particular region of anatomy to be registered, e.g., mandible.

The subtraction service presented in this work is an application of parametric registration of X-ray images, and uses an automatic, intensity-based registration method. Furthermore, a real encoding and distributed evolutionary algorithm is used to find the projective transformation that aligns the images. These will be analyzed in the following section, Section 3, Methodology.

2.1. Problem formulation

From a computational point of view, this is an optimization problem that involves finding the geometric transformation that maximizes the similarity between two images. From a clinical point of view, the problem is to determine whether the proposed automatic system can replace the manual alignment process that is performed –by experts– in the assessment of post-surgical bone mineralization.

3. METHODOLOGY

In this section we will review the methodology followed in this research. This includes the acquisition and selection of the images, their preprocessing, the geometrical transformations used, the chosen interpolation criterion, and the optimization method applied. These make up the registration method proposed.

3.1. Image acquisition process

For this research, a group of nine patients in post-operative periradicular surgery was selected. Radiographs were taken one and three months after surgery, using a radiographic equipment FIAD, model DR508, serial 5841139. The film holder used was Rinn EndoRay II and the film Kodak InSight Ultraspeed type D, developed with Kodak GBX liquids. Radiographs were taken and developed by different operators, using liquids with different degree of fatigue. Subsequently, the radiographs were scanned with a Hewlett Packard ScanJet 3570, at a resolution of 600 x 600 DPI, producing images of 724 x 930 pixels and 256 gray intensities.

In order to minimize shape distortion of the radiographic images, radiographs were taken using the paralleling technique, also known as *right angle paralleling technique* [26]. According to this technique, the film must be placed as nearly parallel to the long axes of the teeth as possible, keeping the film flat at all times and perpendicular to the rays. This technique was preferred because it produces more accurate and less distorted radiographic images than the bisecting angle technique [27].

3.2. Preprocessing

The cases evaluated were intentionally selected from radiographs taken in daily clinical practice. To correct the problem of intensity differences, the system performs an automatic preprocessing step that consists in equalizing the floating image based on the intensities present in the reference image [28]. This adaptive algorithm calculates the histograms of both images and then evenly distributes the intensities of the floating image according to the intensities found in the reference image, thus enhancing its contrast.

3.3. Geometrical transformations

According to Gröndahl [4], small bone deformations can be modeled appropriately by affine or projective transformations. The radiographs obtained for this work are mostly from the occlusal plane, where should be easy to position the X-ray cone perpendicular to the tooth of interest. However, experimental results [29] showed that the capacity of the algorithm to correctly register images, significantly deteriorated in the presence of very strong misalignments. Further studies allowed us to determine that affine transformations were not enough to properly model the acquisition geometry, and that also rotations in the x and y axes should be taken into account. The projective transformations applied in this work can be defined using homogeneous coordinates such as:

$$\begin{pmatrix} u \\ v \\ w \end{pmatrix} = \begin{pmatrix} a_1 & a_2 & dx \\ a_3 & a_4 & dy \\ a_5 & a_6 & 1 \end{pmatrix} \begin{pmatrix} x \\ y \\ 1 \end{pmatrix},$$
$$\begin{pmatrix} x' \\ y' \end{pmatrix} = \begin{pmatrix} u/w \\ v/w \end{pmatrix} \quad (2)$$

Therefore, the new coordinates (x', y') of pixels (x, y) in the template image, are given by $x' = (a_1x + a_2y + dx)/(a_5x + a_6y + 1)$ and $y' = (a_3x + a_4y + dy)/(a_5x + a_6y + 1)$.

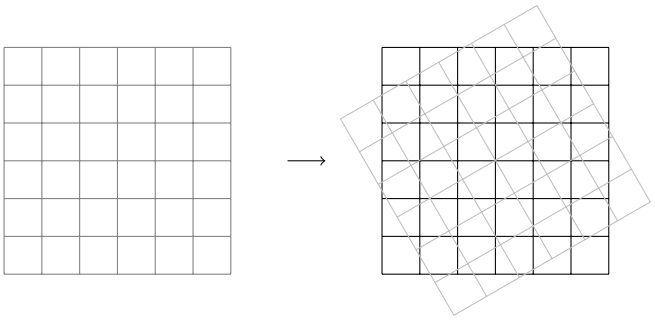

Fig. 1. Original and transformed floating image superimposed to the reference image.

3.4. Interpolation criterion

When transforming an image, by means of rotation or translation for instance, the resulting grid points do not necessarily fall on the points of destination grid (see Figure 1). Therefore, the computation of the intensity of the pixels in the transformed image requires a process of *interpolation*.

The interpolation can be performed using various mathematical functions. Linear interpolation is the least expensive, but its accuracy is very low. Better results can be obtained by interpolating with polynomials of high degree, however the computational cost increases proportionally. In this paper, spline interpolation was used because they use low-degree polynomials, making the computational cost is acceptable, while allowing to achieve good accuracy. Based on the Nyquist-Shannon sampling theorem, Unser [**?**] shows that uniform B-splines are the best discrete representation of a continuous signal. Being uniform, this type of splines have the added advantage that they can be precomputed (for a given image pair) at the beginning of the algorithm, thereby significantly reducing the total processing time.

3.5. Similarity measure

The mutual information measure, successfully applied to multimodal image registration [19, 30], assumes only statistical dependence between image intensities. It treats intensity values in a purely qualitative way, without considering any correlation or spatial information conveyed by nearby intensities. Mutual information tries to reduce entropy and this can be observed as a trend to form intensity clusters in the joint histogram. In the problem of radiography subtraction, since it deals with mono-modal images of natural tissue, the mutual information measure is under-constrained and a functional correlation can be assumed.

The concept of functional dependence, fundamental in statistics, provided us with the framework for the computation of similarity between the two images. To use this concept we consider images as random variables and interpret an image histogram as its probability density function. Furthermore, we consider the 2D histogram of a pair of images as their joint probability density function as proposed in [31]. Thus when a pixel is randomly selected from an image X having N pixels, the probability of getting an intensity i is proportional to the number of pixels N_i in X having intensity i, i.e.,

$$P(i) = \frac{N_i}{N}. \tag{3}$$

In order to define the joint probability density function of an image pair, we consider two images (X, Y) and a spatial transformation T that maps the set of pixels of Y, Ω_y, to the set of pixels of X, Ω_x. Since we are working with digitized radiographs, we can also assume that images X and Y take their intensity values from a known finite set $\mathcal{A} = 0, ..., 255$:

$$X : \Omega_x \to \mathcal{A}, Y : \Omega_y \to \mathcal{A}$$

Now, by applying transformation T to image Y, a new mapping is defined from the transformed positions of Y to $\mathcal{A}$:

$$\begin{aligned} Y_T : T(\Omega_y) &\to \mathcal{A}, \\ \omega &\mapsto Y[T^{-1}(\omega)]. \end{aligned}$$

We now have to find the intensities that a given point of $T(\omega_y)$ simultaneously takes in X and Y_T . Since we are dealing with continuous spatial transformations, points of the grid $T(\omega_y)$ do not, in general, transform to points of the grid ω_x . So, in order to define the joint probability density function of the images, we used the interpolation approach explained below, discarding the points of $T(\omega_y)$ that do not have eight neighbors in ω_x. If we denote by $T(\omega_y)^*$ the subset of accepted points and by $\tilde{X}$ the interpolation of X, we can define the image pair as the following couple:

$$\begin{aligned} Z_T : T(\Omega_y)^* &\to \mathcal{A}^2, \\ \omega &\mapsto \left(\tilde{X}(\omega), Y[T^{-1}(\omega)]\right), \end{aligned}$$

and, in a similar way as we did for a single image in Eq. (3), their joint probability density function as:

$$P_T(i,j) = \frac{Card\left\{x \mid Z_T(x) = (i,j)\right\}}{Card\, T(\Omega_y)^*}. \tag{4}$$

On the other hand, the total variance theorem:

$$Var(Y) = Var\left[E(Y|X)\right] + E_X\left[E(Y|X = x)\right], \tag{5}$$

expresses the fact that the variance can be decomposed as a sum of two energy terms: a first term $Var\left[E(Y|X)\right]$ that is the variance of the conditional expectation and measures the part of Y which is predicted by X, and a second term $E_X\left[E(Y|X = x)\right]$ which is the conditional variance and stands for the part of Y which is functionally independent of X.

Now, based on the previous equation that can be seen as an energy conservation equation, we can define the *correlation ratio* as the measure of the functional dependence between two random variables:

$$\eta(Y|X) = \frac{Var\left[E(Y|X)\right]}{Var(Y)}.$$

Unlike the *correlation coefficient* which measures the *linear* dependence between two variables, the correlation ratio measures the *functional* dependence. The correlation ratio takes on values between 0 and 1, where a value near 1 indicates high functional dependence. Then, for a given transformation T, in order to compute $\eta(Y_T|X)$ we can use the following equation:

$$1 - \eta(Y_T|X) = \frac{E_X\left[Var(Y_T|X = x)\right]}{Var(Y_T)},$$

that by means of Eq. (4) and Eq. (5) can be expressed as:

$$1 - \eta(Y_T|X) = \frac{1}{\sigma^2}\sum_i \sigma_i^2 P_{x,T}(i),$$

where

$$\sigma^2 = \sum_j j^2 P_y(j) - m^2, \;\; m = \sum_j j P_y(j),$$

and

$$\sigma_i^2 = \frac{1}{P_x(i)}\sum_j j^2 P(i,j) - m_i^2, \;\; m_i = \frac{1}{P_x(i)}\sum_j j P(i,j).$$

The correlation ratio measures the similarity between two images and is assumed to be maximal when the images are correctly aligned.

3.6. Optimization method

As discussed in Section 1, any registration method is determined by the geometric transformation, the similarity measure and the optimization scheme used.

The geometric transform used determines the set of parameters to find. As projective transformations were used, the parameters to find are the translation in both axes, the rotation angles with respect to the XYZ-axes and the scaling factor.

Usually, the similarity between two images is calculated based only on the intensity values. However, since we are dealing with natural tissue imaging and both images from the same modality (X-rays), we can assume the existence of a functional correlation between them, thus the correlation ratio [31] is the best option for this task.

The problem of finding the global maximum of a function, whose mathematical formulation is not known, presents several computational challenges. In general, standard numerical methods such as the Downhill Simplex method or Powell's method converge quickly to the solution when the objective function varies smoothly [32]. Otherwise they are very sensitive to the initial conditions chosen and therefore tend to be trapped in local extrema that are not optimal. An alternative is to use evolutionary algorithms that are computationally expensive but that also are, as we will see below, inherently parallel.

Different approaches have been proposed for correcting such geometrical distortions. It goes from manual correction to different devices used to ensure a consistent geometric projection which can be reliably reproduced over time. In daily medical practice, however, devices for adequate patient fixation are not available to clinicians, a drawback that has not allowed the application of this method to the series of routine examinations needed for progression estimation of lesions or treatments. In fact, since most clinicians do not pay attention to this issue, radiographic examinations generally produce strong geometrical distortions which makes it inappropriate to apply conventional correction approaches. Under these circumstances, standard numerical techniques for extrema searching like the Powell's [21] method or the Downhill Simplex method [22] usually yield irrelevant results.

In this section, an entirely automatic method is proposed for spatial radiographic alignment in those cases where a considerable amount of distortion is presented. The process starts by selecting one of the two images as the reference while the other is considered to be the floating image. Afterwards, illumination differences are eliminated by means of the equalization algorithm explained before. Consecutive projective transformations are then performed on the floating image, and the outcome is compared to the reference image using the correlation ratio as the similarity measure.

Conventional registration approaches have been successfully used in those situations where the patients head has been appropriately fixated, therefore producing images with little distortions. However, anatomical variations either from patient to patient or for the same patient in two different moments, have been a major inconvenience for radiographic subtraction to become an applicable method in routine evaluations. Our computational problem can be redefined, therefore, as a multi-parametric search in a highly irregular space of possible transformations, for which conventional approaches have a high probability of remaining trapped in local extrema.

Evolutionary algorithms (EA) represent a subset of evolutionary computation and use mechanisms inspired by biological evolution: recombination, mutation, and selection. By simulating the natural selection process, where the fittest individuals are more likely to survive, these algorithms can be used to find approximate or even exact solutions to optimization problems. Candidate solutions to the optimization problem play the role of individuals in a population, and the fitness function determines the environment within which the solutions live, also known as the *cost function*.

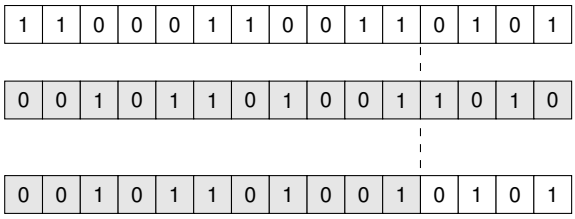

Fig. 2. An example of one-point crossover when using binary encoding. Once a *crossover point* is randomly chosen, the offspring chromosome will consist of a combination of the two parent substrings. This mechanism can be used to produce one or two offsprings.

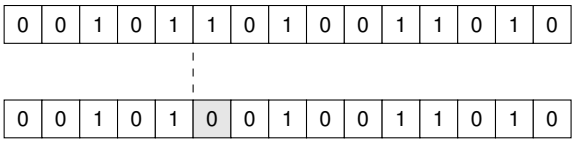

Fig. 3. An example of mutation when using binary encoding. A *mutation point* is randomly chosen and then the allele in that position is inverted.

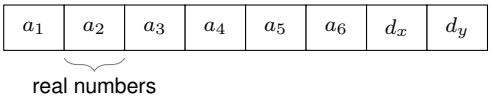

Fig. 4. Real-number encoding of the chromosome used in both evolutionary algorithms.

Evolutionary algorithms are implemented as a computer simulation in which a population of abstract representations of candidate solutions evolves towards better solutions. These representations are called *chromosomes* (or the genotype of the genome), and the candidates are called *individuals* or *phenotypes*. Traditionally, individuals are represented as binary strings, but as we shall see, real number encoding is also possible. The evolution usually starts from a population of randomly generated individuals and occurs in generations. In each generation, the fitness of every individual in the population is evaluated, multiple individuals are stochastically selected from the current population, recombined and mutated to form a new population. The new population is then used in the next iteration of the algorithm. Commonly, the algorithm terminates when either an adequate fitness level has been reached, a maximum number of iterations has been reached, or, as in our case, the available computational time is exausted.

Despite their computational cost, evolutionary algorithms have been chosen over standard numerical methods because of their strong immunity to local extrema, their intrinsic parallelism and robustness, as well as their ability to cope with large and irregular search spaces. In this section we compare two simple evolutionary algorithms categorized as *parallel iterative* [33]: a Genetic Algorithm (GA) and Differential Evolution (DE). Genetic algorithms are attributed to Holland (1975) [23] and Goldberg (1989) [34], while evolution strategies were developed by Rechenberg (1973) [35] and Schwefel (1995) [36]. A good and diverse set of GA examples is synthetized in Chambers [37], while a practical approach to Differential Evolution can be found in [25]. Both approaches mimic Darwinian evolution and attempt to evolve better solutions through recombination, mutation, and selection. However, some distinctions do exist. DEs are very effective in problems of continuous functions optimization, in part because they use real encoding and arithmetic operators. Since GAs generally encode parameters as binary strings and manipulate them with logical operators, they are more suited to combinatorial optimization.

Upon analyzing some of the most relevant works in this area [38, 39, 40], it can be concluded that when using evolutionary algorithms the most crucial aspects refer to the selection of the *coding scheme* and the design of the *fitness function*.

Traditionally, solutions (chromosomes) are represented in binary as strings of 0s and 1s, but other encodings are also possible. Figures 2 and 3 clearly show one the advantages of binary encoding: the crossover and mutation mechanisms are very simple to implement. However, all researchers in the field seem to agree that for this kind of optimization problem, *real-number encoding* performs better than both binary and Gray encoding [41]. Accordingly for the problem at hand, in both evolutionary algorithms the chromosome has been coded as eight floating point numbers representing the set of parameters used in the projective transformation (see Fig. 4).

The initial population includes an individual that is either the null transformation or the center of mass transformation, according to their respective fitness. The rest of the population is generated randomly within the search space.

The fitness of each individual, indicating the similarity between the transformed image and the reference image, is then computed using the correlation ratio previously described. Selection in the GA is performed as follows. The fittest ten percent of the population is selected to be part of the next generation, a facet known as *exploitation*. The rest of the individuals are the result of either crossver ($p_c = 0.85$ in our implementation) or random selection. In the case of crossover, the parents of each new offspring are selected by tournament (5% the size of the population) from the current population. Finally, leaving unmodified the individuals selected by elitism (the evolution history), new candidate individuals are mutated according to a predetermined probability ($p_m = 0.21$), known as the *exploration* characteristic.

Crossover in the GA is performed applying a convex oper-

ator as suggested by Davis in [42]. The genes of an offspring chromosome are then the result of a convex interpolation of the parameters of the two mates. A mutation operator is applied to guarantee that the probability of searching a particular subspace of the problem space is never zero. This prevents the algorithm from becoming trapped in local extrema [34]. The mutation operator used, known as *real number creep*, sweeps the individual adding or subtracting a Gaussian distributed random noise to each parameter [42]. The creep operator implemented can be seen as a neighborhood search that looks in the vicinity of a good solution, to see if a better one exists.

By contrast, in DE all individuals undergo mutation, recombination, and selection. Mutation starts by randomly selecting three individuals (*vectors* in DE terminology) and adding the weighted difference of two of the vectors to the third, and hence the name *differential mutation*. The resulting vector is called the *donor* vector. For recombination, a *trial* vector is developed from the elements of the target vector and the elements of the donor vector. The elements of the donor vector enter the trial vector with a given probability ($C_r = 0.5$). In this step, to ensure that the trial vector results effectively different from the target one, one of the elements of the donor vector is selected at random and entered directly into the trial vector. Finally, target and trial vectors are compared and the one with the higher similarity measure is selected to be part of the next generation.

This process is repeated in both algorithms until some stopping criterion is reached. In our example, given that we receive a large variety of cases, a predetermined similarity measure is ineffective as the only stopping criterion. For this reason, the actual stopping criterion in our case is given by a maximum number of allowed iterations that is computed as follows. The available processing time span is about 12 hours, and since each iteration takes an average of 250 ms, we can make an estimate of the overall number of iterations that can be performed from one day to the next. Also, according to tests carried out with synthetic images, it has been determined that to obtain acceptable results, at least 200 iterations are required. Based on these considerations and the number of images to be processed, we precompute the number of times the algorithm can be executed for each pair of radiographs in the daily batch. The algorithm is then executed the maximum number of times possible and the best result obtained is the one used for the subtraction process.

4. RESULTS

To establish the optimal resolution when scanning the radiographs, different standard values were tested. At a resolution of 300 DPI, the resulting images (362 x 465 pixels) do not provide the level of detail needed for manual registration by the experts. At a resolution of 1200 DPI, the resulting images (1448 x 1860 pixels) provide an excellent level of detail, but contain 16 times the number of pixels at 300 DPI, so the processing time is increased by a factor of about 20. Based on the ability of the experts to assess the information present on the radiographs, it was determined that the most appropriate resolution is 600 DPI. At this resolution, the resulting image size (724 x 930 pixels) allows manual registration and yet can be processed automatically in a reasonable time (less than 40s).

In the early stages of the research, several automatic registration tests were performed using the digitized radiographs without any additional processing. The equalization of intensities proved to be a crucial prerequisite for a successful registration. It is performed only once, at the beginning of the process, and takes 25 milliseconds on a personal computer with a 2.66 GHz Intel Pentium D.

The interpolation by B-splines is appropriate with regard to the quality of the resulting images, although it is an expensive method from the computational point of view: the processing time for a digital radiograph is 1100 milliseconds, compared to 160 milliseconds that takes using bilinear interpolation.

As mentioned before in Section 1, since we are working with occlusal plane radiographs, the deformations present in the images could be corrected using affine transformations. However, in those studies where it is difficult to position the X-ray cone perpendicular to the tooth of interest, as in the case of X-ray images from the upper jaw, it would be necessary to use projective transformations. To avoid losing generality, and since affine transformations are a special case of projective transformations, we decided to use the latter.

4.1. Algorithms Validation

To validate the correctness of the evolutionary algorithms implemented, two sets of experiments were conducted. In both cases, the algorithms were compared to a standard numerical method, the Downhill Simplex method devised by Nelder and Mead. This method was chosen because of its ease of implementation and because, amid the standard numerical optimization methods, it is the least sensitive to initial conditions. First, a series of synthetic images was created by applying a set of known transformations to ten reference radiographs. Then the transformed images were registered to the original ones to verify the ability of each algorithm to find the original values used in the transformation. In the second batch of experiments the algorithms were evaluated with pairs of images obtained from real radiographs.

4.1.1. Experiments with synthetic images

The set of synthetic images was created by applying the transformations shown in Table 1, using a reliable image processing program. The algorithms were executed ten times for each pair of reference and template images. The GA and DE algorithms were executed on the computational grid, while the Downhill Simplex implementation was executed on a single machine of the same grid, using its full processor capacity.

Table 1. Some combinations of rotation, scaling, and translation applied to the set of synthetic images.

	θ_x	θ_y	θ_z	T_x	T_y	SF [a]
1	1	1	1	10	10	0.8
2	10	1	1	10	10	0.8
3	10	10	1	10	10	0.8
4	10	10	10	10	10	0.8
5	10	10	10	100	10	0.8
6	10	10	10	100	100	0.8
7	1	1	1	10	10	1.2
8	10	1	1	10	10	1.2
9	10	10	1	10	10	1.2
10	10	10	10	10	10	1.2
11	10	10	10	100	10	1.2
12	10	10	10	100	100	1.2

[a] SF: scale factor, angles expressed in degrees and translations in pixels.

Table 2. Values found by the Downhill Simplex algorithm.

	θ_x	θ_y	θ_z	T_x	T_y	SF	CR [a]	$Err\,\%$
1	0.91	0.88	1.17	8.55	8.78	0.88	0.67	12.5
2	12.32	1.15	0.76	8.75	11.74	0.81	0.61	15.6
3	11.15	8.16	0.91	13.28	10.98	0.83	0.64	14.2
4	13.98	7.75	12.24	7.34	8.68	0.79	0.50	21.0
5	8.11	8.12	10.83	76.16	7.74	0.78	0.60	15.8
6	7.98	10.71	12.77	91.21	129.05	0.67	0.56	18.2
7	1.11	0.96	0.87	8.15	10.78	1.08	0.71	10.7
8	7.12	0.95	0.82	9.05	10.54	1.04	0.65	13.3
9	7.67	12.98	1.31	6.55	8.13	1.42	0.40	25.9
10	8.73	9.01	11.96	13.34	12.26	1.41	0.53	19.3
11	10.98	12.85	7.77	87.14	7.76	1.01	0.55	18.6
12	11.96	6.72	6.11	111.17	132.32	1.39	0.42	25.1

[a] CR: correlation ratio.

For the set of synthetic images, the transformation values and correlation ratio obtained by the Downhill Simplex method, the Genetic Algorithm, and Differential Evolution are presented in Table 2, Table 3, and Table 4, respectively.

From these results, it can be concluded that for deformations in the expected range, both evolutionary algorithms outperform the Downhill Simplex algorithm and provide clinically acceptable registration accuracy. Moreover, Table 4 shows that the DE algorithm produces the most accurate results.

4.1.2. Experiments with real images

For the second experiment, a group of ten intra-oral radiograph pairs, taken on different occasions, was randomly selected from an unrelated study of periodontal therapy. No film holders or any other fixation device were mechanically coupled to the cone of the X-ray machine. Radiographs were digitized in a HP 3570 scanner using a transparent material adapter at a resolution of 600 $\times$ 600 DPI, producing 724 $\times$ 930 pixel images.

Table 3. Values found by the Genetic Algorithm.

	θ_x	θ_y	θ_z	T_x	T_y	SF	CR	$Err\,\%$
1	0.98	1.03	0.96	9.65	10.15	0.81	0.87	2.5
2	11.01	0.99	1.01	9.43	9.96	0.82	0.85	3.5
3	9.47	10.03	1.03	9.15	11.37	0.82	0.81	5.6
4	8.69	8.98	9.21	9.99	10.50	0.79	0.79	6.3
5	10.1	10.93	11.10	96.04	13.34	0.78	0.72	10.2
6	8.76	11.23	11.52	115.88	96.13	0.82	0.71	10.4
7	1.03	1.09	0.99	10.12	10.35	1.21	0.86	3.1
8	9.44	0.95	0.89	9.53	9.66	1.16	0.81	5.5
9	10.91	9.78	1.11	9.01	11.00	1.23	0.77	7.7
10	9.62	10.12	10.52	11.08	11.10	1.22	0.79	6.4
11	9.63	9.21	10.09	92.77	12.96	1.32	0.73	9.5
12	12.08	10.23	8.91	93.49	108.65	1.34	0.72	10.0

Table 4. Values found by Differential Evolution.

	θ_x	θ_y	θ_z	T_x	T_y	SF	CR	$Err\,\%$
1	0.99	0.99	1.02	9.66	9.78	0.82	0.88	2.0
2	10.05	0.98	0.99	9.55	9.36	0.81	0.87	2.6
3	9.77	10.02	1.03	10.1	10.99	0.83	0.85	3.4
4	9.01	9.57	9.52	9.98	10.02	0.80	0.85	3.5
5	10.2	9.78	11.1	95.99	11.34	0.81	0.81	5.6
6	9.06	10.55	9.43	92.77	117.31	0.82	0.76	7.9
7	0.98	0.97	1.01	9.88	10.02	1.10	0.87	2.6
8	10.2	0.97	0.91	10.53	9.87	1.15	0.84	4.1
9	9.85	10.15	0.97	10.9	10.7	1.19	0.84	3.8
10	10.34	9.88	9.68	10.95	9.15	1.18	0.83	4.6
11	10.65	10.37	9.76	109.01	9.13	1.19	0.82	5.2
12	9.19	9.39	10.91	110.56	92.28	1.17	0.77	7.4

Table 5. DS-GA-DE performance comparison.

Property	DS	GA	DE
Similarity measure (avg)	0.63	0.81	0.83
Execution time (avg)	$52s$	$50s$	$49s$
Number of CPUs	1	120	120

Even though acquisition conditions are standardized as much as possible, illumination differences are inevitable. Thus, the histogram of the template image is equalized by using the reference image luminances. This transformation first computes the histogram of each image and then luminances are homogeneously distributed in the template image according to the levels found in the reference image. The properties compared in this experiment were accuracy, in terms of the similarity measure obtained, and efficiency, in terms of execution time and use of resources. All algorithms were coded in the same programming language and use the same routine to compute the correlation ratio between the transformed and reference images. For this comparison, the three algorithms were also executed ten times for each pair of radiographs. A summary of the results obtained is presented in Table 5:

As expected, the Downhill Simplex method appeared to be very sensitive to the initial parameters and not always converged to the global optimum. While in some executions it obtained better results than the EAs, in other executions it produced meaningless values and this is reflected in the low overall accuracy shown in Table 5. Again, the DE algorithm consistently outperformed the GA and for that reason it is the algorithm currently used in production. It is also important to note that the computational grid, used to run the EAs, only uses the free CPU cycles of the computers that make it up.

Fig. 5 shows a pair of radiographs to be subtracted (top row). The bottom row displays subtraction without geometric correction on the left and with correction on the right. Null intensity level is shifted to 128 in order to make tissue changes easily observed. In this particular example, it can be appreciated that the match is precise enough to make objective measurements despite the fact that in the second radiograph, the fifth tooth (from left to right) is nearly hidden. The small spot, possibly an artifact, that appears in both images is observed in the resulting image in white, indicating that new tissue developed. In this image it can also be observed that a difference appears at the root of the third tooth which corresponds to new tissue developed after treatment. These changes are impossible to observe in the raw difference image (bottom left). Similarly, in this image the bone pattern is blurred and impossible to recognize, while in the resulting image the trabecular bone pattern is clear. For the entire set of test images, matching has been visually assessed by two experts in the field. They

Fig. 5. The upper row shows the two images to subtract. Bottom row shows the subtracted images: left without geometrical correction and right after automatic correction.

judged that the alignment was sufficiently accurate to get objective measurements while maintaining acceptable computation times.

For the evolutionary algorithms used, several thousands of experiments were performed in order to guarantee a complete analysis of the parameter space. An experiment is the execution of the algorithm with a particular set of images and parameters, i.e. population size, tournament size and genetic operators probabilities. In this task the grid became an essential tool and allowed us to achieve a second level of parallelism. The first analysis was conducted to determine two basic parameters of the algorithm: population size and selection scheme used to choose the parents for crossover. The experiments showed that the optimum population size for this problem is 120. Two common selection options are tournament selection and elitism. In tournament selection of size N, N individuals are selected at random and the fittest is chosen. Elitism is a particular case of tournament selection where the size of the tournament equals the size of the population, so the best individual is always preserved. For this problem, tournament selection of size 12 is the best option for selecting the parents for a new generation. The other parameters analyzed

were the crossover and mutation probabilities. The combination of probabilities that yielded the best results were 0.76 and 0.18 respectively.

Another advantage of the DE algorithm over the GA is that it only uses two parameters: the scale factor F, that controls the rate at which the population evolves, and the uniform crossover probability C_r. This makes the analysis of the parameter space simpler and therefore tuning of the algorithm becomes easier. The values found for the DE algorithm are $F = 0.5$ and $C_r = 0.5$.

4.1.3. Experts validation

A second kind of experiment was conducted to compare the results obtained by the automated system with the results obtained by experts in the area, using a manual registration system. For this, the experts used an interactive graphical service in which they can visualize and manipulate, using mouse and keyboard, the images to register. As the expert is applying the different transformations, the application will calculate the corresponding correlation rate. This allows the expert to determine the direction in parameter space in which the correlation rate increases. At any moment, the expert can choose to automatically register the images and then compare the result with the current manual registration.

For this set of experiments we were assisted by four maxillofacial surgeons who used the manual registration system. The transformation parameters used by the experts for the registration were stored and compared statistically with those found by the automated system.

The results show that the automatic method achieves, in all cases, better similarity measures than those obtained by the different experts. This is mainly due to the fact that the automatic method uses all the image pixels to achieve the best registration, which does not necessarily mean that the registration is qualitatively better than that done by the expert. The expert, by contrast, focuses attention on the region of interest, therefore, even when getting a lower similarity measure, this region can be better registered. Moreover, the qualitative assessment made by experts from the automatic records, ensures that the proposed system is able to largely replace, and thus avoid the experts the expensive process of manual registration. In cases where the automatic method obtains a registration that is not optimal from a qualitative standpoint, the expert can still use the interactive system, which includes the required tools for manual registration, to improve the registration of the region of interest. One might think then in a semi-automatic, where the expert would mark prior to registration automatic, the region of interest. However, in most cases the automatic method achieves an appropriate registry, thus saving valuable time to the expert, especially when it comes to evaluating multiple cases.

4.2. The subtraction service

The medical imaging community has a growing need for Internet-aware tools that facilitate interaction with remote data in a collaborative way. Such medical imaging data typically requires special-purpose tools that come in the form of stand-alone and non-portable applications, i.e., software to be manually installed and maintained on a local computer. This is possible provided there is an available binary version for the particular platform in use, or the source code is publicly obtainable and the user is responsible for gathering the required libraries and tools, and compiling the source code. There is also a growing need in the medical imaging community for Internet-aware software tools that facilitate collaborative data analysis and visualization. Research projects and clinical studies require a medium for a geographically dispersed scientific and clinical community to interact and examine medical imaging data via the Internet. Additionally, health care and medical research rely increasingly on the use of computationally intensive algorithms.

The service-oriented model proposed has many advantages over the stand-alone application model. First and foremost, it avoids the user having to manually install the software. All that is needed is a standard web browser and an Internet connection: the platform dependency is no longer an issue. In addition, updates are made on the server side and automatically propagate to all service users. By having redundant and clustered servers it is possible to attain high data availability, something difficult -if indeed possible- with a personal workstation. Finally, and most important, the service-oriented paradigm leverages interdisciplinary and collaborative work, one critical success factor in biomedical practice and research. This section will present a service-oriented model for medical imaging via the Internet. Services are accessed via a standard web browser, however the essential tools also work off-line. This is accomplished by using a local server and a local database, and synchronizing data when the user goes back online.

The proposed architecture for this model is basically an enhanced version of a standard client-server architecture (please, refer to Figure 6). The difference lies in the addition of a local server that allows for the basic services to keep functioning without an active Internet connection. The proxy component is responsible for providing the essential functionality when the user is disconnected from the Internet, and for synchronizing data with the server when the connection is active again. To accomplish this, the local server is connected to a lightweight relational database engine that allows the client application to store, search and recover data using the structured query language (SQL).

On the client side, services are accessed using a standard web browser. In our implementation, all services use a digitally-signed Java browser extension ("applet") that takes care of the installation of the local server and other required

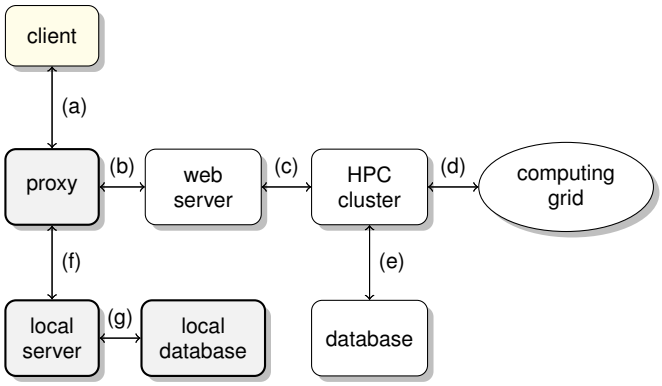

Fig. 6. Overall architecture of the subtraction radiography service, showing the technologies used for communication between neighbouring components: (a) plain Java objects (POJO), (b) HTTP, HTTPS, sockets TCP/UDP, (c) Job Submission Description Language (XML) over sockets TCP, (d) JavaSpaces API, (e) Java Database Connectivity (JDBC), (f) sockets TCP, (g) JDBC.

Fig. 7. Graphical user interface for the radiography subtraction service.

tools such as the database engine (e.g. Apache Derby) and OpenGL[1] libraries. Additionally, the applet provides the tools for visualization, manipulation and light processing tasks such as image reconstruction and geometric transformations. On the server side, and behind a pool of web servers, there is a high-availability cluster that provides access to the computing grid (HPC). The cluster is based on the Sun HPC stack [43], including components such as the Lustre [44] file system, Sun Grid Engine [45] for distributed resource management, Ganglia [46] and Nagios [47] for system monitoring. To avoid the existence of a single-point of failure (HA), the cluster uses a replicated, distributed, transactional tree-structured cache. The cache service has been built upon the Terracotta [48] platform, which in turn uses peer-to-peer technologies to provide the basic services.

The subtraction service provides two modes of operation: an *interactive mode* and a *batch mode*. In the first mode, the user loads the images to register, and interactively drags, rotates and scales the template image to align it manually. Once registered, the images can be subtracted and the difference visualized. Since this is a lightweight operation, it is carried out completely on the client side. However, the user can choose to register the images automatically. In this case, the images are uploaded to the server (if not already there), and then registered by the aforementioned distributed algorithm. Once this task is finished, the parameters of the projective transformation are sent back to the client application for visualization.

With the help of the local server and database, the interactive mode keeps working even without an active Internet connection, provided the images reside in the local machine. This is what happens most of the time, either because the images were produced on the local machine, or because they were previously downloaded from the server. The synchronization process is the responsibility of the so called *proxy* element that the client application actually communicates with: it uploads the locally digitized images to the server, and downloads the images stored on the server to the corresponding client computers. The automatic mode does require an active Internet connection to benefit from the HPC cluster. Otherwise, it will try to execute using the available local resources.

In practice, the service is mostly used in the second or *batch mode*. In this mode the set of radiographs taken daily are digitized and uploaded to the service server where they are registered automatically by the same evolutionary algorithm. The job of the master process, executed in the cluster, is to generate the initial populations and send them to the computing grid for evaluation. Since the fitness of each individual can be evaluated independently from the others, this task is performed in parallel on the grid. Once evaluated, each population is collected by the corresponding master process that applies the genetic operators (mutation, recombination, selection), produces a new population and sends it again to the grid for evaluation. The process repeats until the stop conditions are met. The optimal transformations are then stored in the server database and sent to the client applications for visualization.

The use of Java and Internet technologies in medical imaging is not new. These technologies have been used in radiology teaching files, to access information in multimedia integrated picture archiving and communication systems (PACS), and for teleradiology purposes. However, all known approaches seem to assume the existence of a stable and reliable Internet connection, and this is not always possible.

[1] OpenGL is a registered trademark of Silicon Graphics Inc.

5. DISCUSSION

In this article, we have reviewed the main aspects involved in the task of medical image registration. Through a simple yet real case study, we have seen one effective way to build a high performance computational grid that benefits from an existing computational infrastructure and open software tools. The computational grid provides an image registration service that has proved capable of greatly lowering the burden of manual work to the experts.

The framework used is based on a loosely-coupled architecture and asynchronous communications. Using a service-oriented architecture that provides a shared and distributed memory space and other essential services (publication, discovery, transactions, leasing), we have implemented a general-purpose computing grid and shown its application in medical imaging. The computing grid is most appropriate for the parallel execution of computationally intensive jobs that can be divided in multiple independent tasks. Other crucial aspects, like security, storage management, and general system administration, are out of the scope of this chapter and have been omitted. However, it is worth noticing that these are essential aspects that in research and clinical environments have to be properly addressed in order to provide secure and reliable medical imaging services.

To demonstrate the applicability of the computing grid in a real situation, we have presented the case study of automatic digital subtraction. In this situation, we evaluated two evolutionary algorithms as the search strategy to solve an expensive optimization problem. This is to find a global maximum of an unknown function that measures the similarity between two given images. In this evaluation, i.e., for this particular problem, differential evolution proved to be more performant and reliable than the genetic algorithm. The global structure of the algorithm is iterative, but since individuals in a population can be evaluated independently from the others, the most time-consuming stage of the algorithm is computed in parallel.

The high computational cost of the evolutionary algorithms in use was addressed by developing a distributed implementation. This implementation exploits the computational power of a big set of personal computers arranged in a low cost computational grid and a small HPC cluster. Since it can be deployed over an existent computational infrastructure, this approach can be affordably implemented in institutions with a low budget, like public and university hospitals.

The proposed service-oriented model for medical imaging is feasible and useful in research and clinical scenarios. The implemented framework allows doctors to use up to date medical imaging techniques and high-performance computing power in routine clinical studies, by means of a standard web browser and without specialized training. Furthermore, the framework allows for new services to be obtained from the integration of existing services with different dynamics, such as 2D/3D/4D, and video processing tools.

The architecture in use is currently evolving towards a *cloud computing* model, in which the common theme relies on integrated services over the Internet to satisfy the clinician computing needs. Regarding the algorithms used in registration, current and future work is related to further exploring hybrid evolutionary algorithms such as those presented in [49, 50, 51], their possible application to the 3D curvature-based registration algorithm proposed in [52, 53, 54], their distribution and parallelization.

6. REFERENCES

[1] L. Lin, P. Gaengler, and K. Langeland, "Perirradicular curetaje," *International Endodontic Journal*, vol. 29, pp. 220–227, 1996.

[2] P. N. Abramowitz, H. Rankow, and M. Trope, "Multidisciplinary approach to apical surgery in conjunction with the loss of bucal cortical plate," *Oral Surgery, Oral Medicine, Oral Pathology, Oral Radiology, and Endodontology*, vol. 77, no. 5, pp. 502–506, 1994.

[3] A. H. Gartner and S. O. Dorn, "Avances en ciruga endodntica," *Dental Clinics of North America*, vol. 36, no. 2, pp. 357–378, 1992.

[4] H. Gr´ondahl, K. Gr´ondahl, and R. L. Webber, "A digital subtraction technique for dental radiography," *Oral Surgery*, vol. 55, pp. 96–102, 1983.

[5] A. Parashis, "Comparison of two regenerative procedures-guided tissue regeneration and demineralized freeze-dried bone allograft-in the treatment of intrabony defects: A clinical and radiographic study," *Journal of Periodontology*, vol. 69, no. 7, pp. 751–758, 1998.

[6] Eastman Kodak Company, "Los rayos x en odontología," 1964.

[7] J. W. Harrison and K. A. Jurosky, "Wound healing in the tissues of the periodontium following periradicular surgery," *Journal of Endodontics*, vol. 17, no. 9, pp. 425–435, 1991.

[8] V. Byrd, T. Mayfield-Donahoo, M. Reddy, and M. Jeffcoat, "Semiautomated image registration for digital subtraction radiography," *Oral Surgery, Oral Medicine, Oral Pathology, Oral Radiology, and Endodontology*, vol. 85, no. 4, pp. 473–478, 1998.

[9] H. Gr´ondahl, K. Gr´ondahl, T. Okano, and R. L. Webber, "Statistical contrast enhancement of subtraction images for radiographic caries diagnosis," *Oral Surgery*, vol. 53, pp. 219–223, 1982.

[10] F. Pernus A. Fidler, B. Likar and U. Skaleric, "Influence of developer exhaustion on accuracy of quantitative digital subtration radiography," *Oral Surgery, Oral Medicine, Oral Pathology, Oral Radiology, and Endodontology*, vol. 90, no. 2, pp. 233–239, 2000.

[11] E. O. Delano, D. Tyndall, J. B. Ludlow, M. Trope, and C. Lost, "Quantitative radiographic follow-up of apical surgery: a radiometric and histologic correlation," *Journal of Endodontics*, vol. 69, no. 7, pp. 420–426, 1998.

[12] E. C. Ekberg, A. Petersson, and M. Nilner, "An evaluation of digital subtraction radiography for assessment of changes in position of the mandibular condyle," *Dentomaxillofacial Radiology*, vol. 27, pp. 230–235, 1998.

[13] P. V. Nummikoski, T. S. Martinez, S. R. Matteson, W. D. McDavid, and S. B. Dove, "Digital subtraction radiography in artificial recurrent caries detection," *Dentomaxillofacial Radiology*, vol. 29, no. 2, pp. 59–64, 1992.

[14] A. Wenzel, "Effect of manual compared with reference point superimposition on image quality in digital subtraction radiography," *Dentomaxillofacial Radiology*, vol. 18, pp. 145–150, 1989.

[15] J. B. Ludlow and C. P. Peleaux, "Comparison of stent versus laser-and cephalostat-aligned periapical film-positioning techniques for use in digital subtraction radiography," *Oral Surgery*, vol. 77, no. 2, pp. 208–215, 1994.

[16] Rueckert D, *Non-rigid Registration: Concepts, Algorithms and Applications*, chapter 13, pp. 281–301, Biomedical Engineering. CRC Press, Florida, FL, 2001.

[17] Lester H and Arridge SR, "A survey of hierarchical non linear medical image registration," *Pattern Recognition*, vol. 32, no. 1, pp. 129–149, 1999.

[18] Farag AA, Yamany SM, Nett J, Moriarty T, El-Baz A, Hushek S, and Falk R, *Medical Image Registration: Theory, Algorithm, and Case Studies in Surgical Simulation, Chest Cancer, and Multiple Sclerosis*, vol. 3, chapter 1, pp. 1–46, Kluwer Academic/Plenum Publishers, New York, NY, 2005.

[19] Maintz JBA and Viergever MA, "An overview of medical image registration methods," Symposium of the Belgian Hospital Physicists Association (SBPH/BVZF), 1997.

[20] Beutel J, Sonka M, Kundel HL, Fitzpatrick JM, and Van Metter RL, *Medical Image Processing and Analysis*, vol. 2, pp. 447–513, SPIE Press, Belligham, WA, 2000.

[21] Powell M, "An efficient method for finding the minimum of a function of several varialbles without calculating derivatives," *The Computer Journal*, vol. 7, no. 2, pp. 155–162, 1964.

[22] Nelder J and Mead RA, "A simplex method for function minimization," *The Computer Journal*, vol. 7, no. 4, pp. 308–313, 1965.

[23] Holland JH, *Adaptation in natural and artificial systems: An Introductory Analysis with Applications to Biology, Control, and Artificial Intelligence*, The MIT Press, Massachusetts, MA, 1992.

[24] Kirkpatrick S, Gelatt Jr. CD, , and Vecchi MP, "Optimization by simulated annealing," *Science*, vol. 220, no. 4598, pp. 671–680, 1983.

[25] Price KV, Storn RM, and Lampinen JA, *Differential Evolution: a practical approach to global optimization*, Springer, 2005.

[26] O. E. Langland, R. P. Langlais, and J. W. Preece, *Principles of Dental Imaging*, chapter 5, pp. 85–138, Lippincott Williams & Wilkins, 2002.

[27] C. Canalda and E. Brau, *Endodoncia técnica clínica y bases científicas*, Editorial Masson España, 2nd. edition, 2006.

[28] U. E. Ruttimann, R. L. Webber, and E. Schmidt, "A robust digital method for film contrast correction in subtraction radiography," *Journal of Periodontal Research*, vol. 21, pp. 486–495, 1986.

[29] G. Mañana, E. Romero, and F. González, "Distributed genetic algorithm for subtraction radiography," *IEEE International Conference on Image Processing*, vol. 13, pp. 3325–3328, October 2006.

[30] Viola P and Wells III WM, "Alignment by maximization of mutual information," *International Journal of Computer Vision*, vol. 24, pp. 137–154, 1997.

[31] Pennec X, Roche A, Malandain G, and Ayache N, "Multimodal image registration by maximization of the correlation ratio," `http://hal.archives-ouvertes.fr/`, 1998.

[32] W. H. Press, S. A. Teulkolsky, W. T. Vetterling, and B. P. Flannery, *Numerical Recipes in C, The Art of Scientific Computing*, Cambridge University Press, 2nd. edition, 2002.

[33] Bahi JM, Contassot-Vivier S, and Couturier R, *Parallel Iterative Algorithms: From Sequential to grid Computing*, Chapman & Hall/CRC, 2008.

[34] D.A. Goldberg, *Genetic algorithms in search, optimization and machine learning*, Addison-Wesley Professional, 1989.

[35] Rechenberg I, *Evolutionsstrategie - Optimierung technischer Systeme nach Prinzipien der biologischen Evolution*, Frommann-Holzboog, Stuttgart, 1973.

[36] Schwefel HP, *Evolution and Optimum Seeking: The Sixth Generation*, Wiley-Interscience, New York, NY, 1995.

[37] L. Chambers, *The practical handbook of genetic algorithms: Applications*, Chapman & Hall/CRC, 2nd. edition, 2000.

[38] A. E. Eiben and J. E. Smith, *Introduction to Evolutionary Computing*, Springer, Natural Computing Series, 2nd. edition, 2007.

[39] L. M. Schmitt, "Theory of genetic algorithms ii: models for genetic operators over the string-tensor representation of populations and convergence to global optima for arbitrary fitness function under scaling," *Theoretical Computer Science*, vol. 310, pp. 181–231, 2004.

[40] P. F. Hingston, L. C. Barone, and M. Zbigniew, *Design by Evolution, Advances in Evolutionary Design*, Springer, Natural Computing Series, 2008.

[41] M. Gen and R. Cheng, *Genetic Algorithms and Engineering Optimization*, Wiley-Interscience, 2000.

[42] L. Davis, *Handbook of genetic algorithms*, Chapman & Hall/CRC, 2nd. edition, 2000.

[43] "Sun HPC Software," `http://www.sun.com/software/products/hpcsoftware/getit.jsp`.

[44] "Lustre^{TM}," `http://wiki.lustre.org/`.

[45] "Sun Grid Engine," `http://gridengine.sunsource.net/`.

[46] "Ganglia Monitoring System," `http://ganglia.sourceforge.net/`.

[47] "Nagios," `http://www.nagios.org/`.

[48] "Terracotta," `http://www.terracotta.org/platform/`.

[49] Talbi H and Batouche M, "Hybrid particle swarm with differential evolution for multimodal image registration," *IEEE International Conference on Industrial Technology*, pp. 1567–1572, 2004.

[50] C. Grosan, A. Abraham, and H. Ishibuchi, *Hybrid Evolutionary Algorithms*, Springer, 2007.

[51] Lozano M and García-Martínez C, "Hybrid metaheuristics with evolutionary algorithms specializing in intensification and diversification: Overview and progress report," *Computers & Operations Research*, vol. In press, 2009.

[52] B. Fischer and J. Modersitzki, "Curvature based image registration," *Journal of Mathematical Imaging and Vision*, vol. 18, pp. 81–85, January 2003.

[53] B. Fischer and J. Modersitzki, "A unied approach to fast image registration and a new curvature based registration technique," *Linear Algebra and its Applications*, pp. 107–124, 2004.

[54] Modersitzki J, *Numerical Methods for Image Registration*, Oxford University Press, 2004.